The crossover to the "$1/f$" region of solar wind fluctuations.

R. M. Nicol*, S. C. Chapman* and R. O. Dendy†,*

*Centre for Fusion, Space and Astrophysics, Dept. of Physics, University of Warwick, Coventry, CV4 7AL, UK
†UKAEA Culham Division, Culham Science Centre, Abingdon, Oxfordshire, OX14 3DB, UK

Abstract. We present generalized structure function (GSF) analysis of magnetic and velocity field fluctuations measured in situ in the solar wind at ~ 1 AU with the ACE spacecraft. We decompose the fluctuations into directions parallel and perpendicular to the mean local background magnetic field. GSF plots based on these quantities are shown to provide a clear indicator of the spectral break between the inertial range and "$1/f$" range of scaling. In GSF plots, the projected velocity and magnetic field fluctuations track each other closely in the inertial range in both fast and slow solar wind and at solar maximum and minimum. At longer timescales the "$1/f$" range is easily identified, because the magnetic field fluctuations display a flattening of the GSFs (exponents become zero) consistent with a $\sim 1/f$ PSD. The velocity fluctuations on the other hand have GSFs which steepen, consistent with a PSD of $\sim 1/f^{\alpha}$ where α as determined by GSF varies with solar wind speed and solar cycle but is closer to two. The extent of the inertial range determined in this manner differs between fast and slow solar wind streams, and between periods of maximum and minimum solar activity.

Keywords: magnetic fields - solar wind - turbulence- anisotropy - "$1/f$ frequency range"
PACS: 96.50.Ci 96.50.Wx 94.05.Lk 52.35.Ra 89.75.Da

INTRODUCTION

The solar wind carries signatures of coronal dynamics as well as locally generated turbulent phenomena, which span a broad range of scales. *In situ* spacecraft observations of fluctuations in solar wind parameters such as velocity and magnetic field (e.g. in the ecliptic plane [29] and in polar flows [9]) typically reveal an inertial range of turbulence with a "$5/3$" inverse power-law scaling at high frequencies and a flatter "$1/f$"-like scaling range at lower frequencies [19, 4]. The breakpoint between these two ranges is seen to evolve radially [1, 10] suggesting an inertial range of turbulent energy cascade in the solar wind. This inertial range has been extensively studied using timeseries analysis techniques including power spectra [16], probability density functions [18, 28, 2] and generalised structure funtions (GSFs) [11, 8, 33, 6, 25].

The solar wind also has a background magnetic field and is therefore a highly anisotropic plasma environment [31, 27]. Here we will focus on the anisotropy of the fluctuations by using a decomposition with respect to the background magnetic field, and we will take advantage of the long timeseries available from the Advanced Composition Explorer (*ACE*) spacecraft to compare not only fast and slow solar wind streams but also periods of minimum and maximum solar activity. In the inertial range, vector quantities such as *in situ* velocity and magnetic field can be resolved for components both parallel and perpendicular with respect to the background magnetic field $\boldsymbol{B}$. The background magnetic field is dominated by different dynamics, depending on whether large scale $\boldsymbol{B}$ (Parker spiral), [20] or average local $\boldsymbol{B}$, as a function of the scale of the fluctuations [6, 13] is considered. Both cases have been studied in the context of inertial range turbulence. In terms of quantifying scaling however, these approaches are generic and the focus of the present paper is to incorporate these ideas in statistical studies of the "$1/f$" range, since we anticipate that coronal processes and the transport or propagation of coronal structures will depend on orientation with respect to the background magnetic field. The observed scaling would also be anticipated to depend quantitatively on solar cycle and to differ between fast (~ 750 km/s) or slow (~ 350km/s) solar wind streams. We will perform GSF analysis on sufficiently long intervals that they span both the inertial and "$1/f$" ranges. The location of the spectral breakpoint between the inertial and "$1/f$" ranges differs in fast and slow streams [12, 3], presumably because at a given heliocentric distance the turbulence in the slow solar wind has had more time to develop than in the fast solar wind. Furthermore, the crossover between the inertial and "$1/f$" range is much clearer in fast than in slow solar wind. We will see that projecting velocity and magnetic field parallel and perpendicular to $\boldsymbol{B}$, combined with GSF plots, provide a clear indicator of where this crossover occurs. We compare the position of this breakpoint in fast and slow solar wind streams and at periods of maximum and minimum solar activity.

POWER SPECTRAL DENSITY

The ACE spacecraft [34] orbits the Lagrangian point sunwards of the earth ($\sim$ 1AU). For the present analy-

CP1216, *Twelfth International Solar Wind Conference,*
edited by M. Maksimovic, K. Issautier, N. Meyer-Vernet, M. Moncuquet, and F. Pantellini

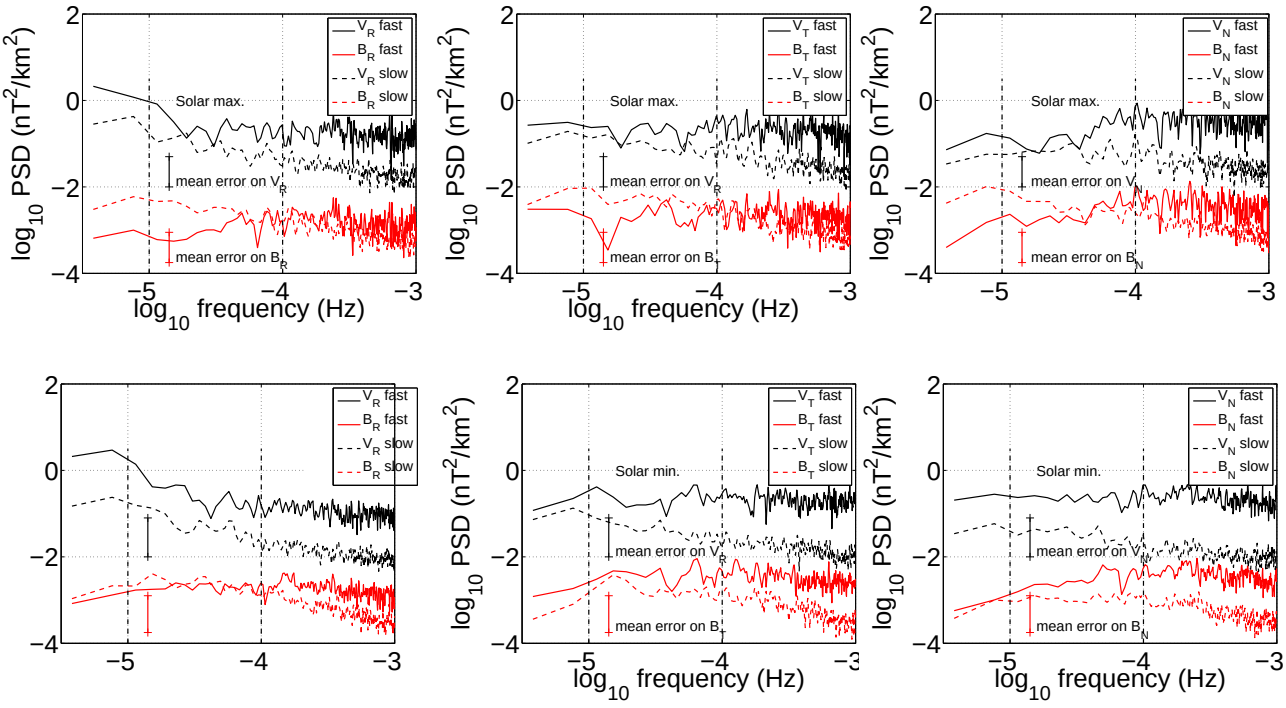

FIGURE 1. (Reproduced by permission of the AAS from [26]) Compensated power spectral density $F(f)/f^{\alpha}$, $\alpha = -1$ for velocity (black) and magnetic field (red) fluctuation components for each of the RTN coordinates in the frequency range $10^{-5.5} - 10^{-3}$Hz. Fast (solid line) and slow (dashed line) solar wind are plotted for solar maximum (upper panels) and solar minimum (lower panels). The dotted vertical lines delimit the frequency range $10^{-5} - 10^{-4}$Hz; this is expected to lie within the "$1/f$" range, with the breakpoint between the inertial and "$1/f$" ranges $\sim 10^{-4}$Hz [17, 10]. Errors are estimated as one standard deviation of the averaged datasets.

sis we study plasma parameters (magnetic field $\boldsymbol{B}$ and velocity $\boldsymbol{v}$) averaged over 64 sec from MAG/SWEPAM [32, 22]: for the year 2007 (solar minimum) and 2000 (solar maximum). This provides datasets of $\sim 4.8 \times 10^5$ samples per year. In order to separate fast and slow solar wind behaviour yet still preserve a dataset with sufficient points to perform GSF in the "$1/f$" dynamic frequency range, we divide the datasets into intervals ($\geq$ 6000 points or 4.5 days) of fast and slow streams, where the cut-off between fast and slow is taken at 450 km/s [12]. These give for 2007 a fast solar wind ensemble of $\sim 7.4 \times 10^4$ points, and a slow solar wind ensemble of $\sim 1.4 \times 10^5$ points, and for 2000 a fast ensemble of $\sim 4.1 \times 10^4$ points and a slow ensemble of $\sim 1.1 \times 10^5$ points. We evaluate the PSD using the original continuous intervals of fast and slow solar wind. We compute the GSF of fluctuations from each single ensemble, however we preserve the time indicators for the data and ensure that the pairs of datapoints from which GSF are constructed are always drawn from within continuous intervals of fast or slow streams.

We first plot the power spectral density $F(f)$ of the components of $\boldsymbol{B}$ and $\boldsymbol{v}$ in RTN coordinates, where R is the sun-spacecraft axis, T is the cross product of R with the solar rotation axis, and N is the cross product of R with T We take continuous intervals of fast and slow solar wind and truncate each to the same length of 6000 datapoints. Each interval is then split up into Hamming windows of $2^{12} = 4096$ points with a 50% overlap. The PSD is composed of an average of the FFTs of these windowed intervals. At lower frequencies, the magnetic field power spectrum $F(f) \sim f^{\alpha}$ shows a spectral slope $\alpha \sim -1$. Plotting $F(f)/f^{\alpha}$, $\alpha = -1$ should therefore give a horizontal line on average. These plots are known as compensated power spectra and are shown for the various solar wind conditions in Figure 1.

Figure 1 covers the expected region of transition in the spectral index of $\boldsymbol{v}$ and $\boldsymbol{B}$ between the inertial and "$1/f$" frequency ranges. However it is difficult to tell precisely whether, for example, the PSD behaviour between 10^{-5}Hz and 10^{-4}Hz really is "$1/f^{\alpha}$, $\alpha = 1$", particularly in the slow solar wind. It also evident from Figure 1 that, in some cases in the "$1/f^{\alpha}$" range, α varies with the solar cycle and with solar wind speed, and that for both $\boldsymbol{v}$ and $\boldsymbol{B}$ the α can vary from one component to another, and between $\boldsymbol{v}$ and $\boldsymbol{B}$. This implies anisotropy in the fluctuations and distinct scaling between $\boldsymbol{v}$ and $\boldsymbol{B}$.

GENERALIZED STRUCTURE FUNCTIONS

We now project the velocity and magnetic field fluctuations into parallel and perpendicular components relative to the background magnetic field (see [26] for details). Other techniques use wavelets to perform the components' decomposition, see for example [30]. The Taylor hypothesis relates spatial and temporal scales; fluctuations over a time lag τ in the velocity (or magnetic field) vector components are defined as $\delta\boldsymbol{v}(t,\tau) = \boldsymbol{v}(t+\tau) - \boldsymbol{v}(t)$. A vector average for the magnetic field direction $\hat{\boldsymbol{b}}(t,\tau) = \overline{\boldsymbol{B}}/|\overline{\boldsymbol{B}}|$ is formed from a vector sum $\overline{\boldsymbol{B}}(t)$ of all the observed vector $\boldsymbol{B}$ values between $t-\tau/2$ and $t+3\tau/2$. It follows that in computing fluctuations over τ, the background field is averaged over $\tau' = 2\tau$, which then defines the minimum (Nyquist) interval necessary to capture wavelike fluctuations [6]. Using this definition of $\hat{\boldsymbol{b}}$, the parallel component is given by $\delta v_{\parallel} = \delta\boldsymbol{v}\cdot\hat{\boldsymbol{b}}$ The perpendicular fluctuation amplitude is given by $\delta v_{\perp} = \sqrt{(}\delta\boldsymbol{v}\cdot\delta\boldsymbol{v} - \left(\delta\boldsymbol{v}\cdot\hat{\boldsymbol{b}}\right)^2)$. Our definition of the perpendicular component is a scalar unsigned quantity, which can be thought of as an angle averaged component in the plane perpendicular to the background field $\overline{\boldsymbol{B}}$. This relies on the assumption of isotropy in this plane which has been tested in [26]. We use these definitions to construct differenced timeseries $\delta v_{\perp}(t,\tau)$, $\delta b_{\perp}(t,\tau)$, $\delta v_{\parallel}(t,\tau)$ and $\delta b_{\parallel}(t,\tau)$ over a range of τ intervals that span both the inertial and "$1/f$" ranges, that is $\tau = 10$ to 1706 minutes.

Scaling can be quantified by computing the GSFs of the fluctuations, $\langle\mid \delta y_\tau \mid^m\rangle$, where $\langle\cdots\rangle$ denotes ensemble averaging, m is the order of the moment and $\delta y_\tau = y(t+\tau) - y(t)$ is the fluctuation in a signal $y(t)$ over a time τ. Assuming weak stationarity and a degree of self-similarity, GSFs can be related to the scale τ of the fluctuation by a scaling exponent $\zeta(m)$, when $S_m = \langle\mid \delta y_\tau \mid^m \rangle \sim \tau^{\zeta(m)}$ whereas the PSD measures $\zeta(2)$ only (e.g.[5]). The scaling exponents $\zeta(m)$ are given quantitatively by the slopes of the GSFs. For practical applications of the GSF analysis to a broad range of datasets, see for example: MHD turbulence simulations - [23, 24]; solar wind turbulence - [11, 8, 6, 25] and geomagnetic indices - [7].

We now apply these methods to the observations. Figure 2 shows the GSFs up to $m = 4$ overplotted for the pairs ($\delta v_{\parallel}$, $\delta b_{\parallel}$) and ($\delta v_{\perp}$, $\delta b_{\perp}$) at solar minimum, and for the pairs ($\delta v_{\perp}$, $\delta b_{\perp}$) at solar maximum. The series is differenced over $\tau = n \times 640$ s for $n = 1$ to 160, that is for a range covering ten to 1706 minutes ($\sim$ 28 hours). We have verified [26] that these GSF are not strongly affected by the presence of poorly sampled outliers in our finite sized sample via the method of [14, 15]. A clear feature common to all the panels in Figure 2 is that the $\boldsymbol{v}$ and $\boldsymbol{B}$ fluctuations track each other closely in the inertial range over a region extending up to, or beyond, 100 min. At larger timescales we see, consistent with the PSD results, that the $\boldsymbol{v}$ and $\boldsymbol{B}$ fluctuations have very different slopes - this is the "$1/f$" range. Specifically, the GSFs for $\delta b_{\parallel,\perp}$ flatten in the $\sim 1/f$ range, consistent with previously reported results based on the PSD [19, 21]. The correspondence between a flat GSF ($\zeta(m) = 0$) and a $\sim 1/f$ PSD is most easily seen if we consider a simple self-affine noise process with PSD $\sim 1/f^{\alpha}$ for which $\alpha = 1+\zeta(2)$, as we take $\alpha \to 1$, $\zeta(2) \to 0$. In fact, for the self-affine fractal noise, $\zeta(m) = \alpha m \to 0$ for all m as seen in Figure 2. The $\delta v_{\parallel,\perp}$ GSFs on the contrary steepen as we cross over into the "$1/f$" range suggestive of scaling processes with exponents distinct from those of $\delta b_{\parallel,\perp}$. These are closer to a value of $\zeta(2) \sim 1$, which, again for a simple noise process, is consistent with PSD$\sim 1/f^2$.

Whilst these results confirm the "$1/f$" scaling of fluctuations in $\boldsymbol{B}$ on long timescales, reported previously (e.g. [19]), they also highlight the distinct scaling of $\boldsymbol{v}$. These GSF plots of fluctuations oriented with respect to the background field clearly show the crossover between the IR and "$1/f$" ranges. We then see that as expected[3, 12], the inertial range is more developed in the slow solar wind compared to fast solar wind. We can also see a solar cycle dependence in the development of the inertial range in the slow solar wind, which extends to much longer timescales at solar maximum. The corresponding solar cycle dependence for the fast solar wind may be due to finite size effects: the dataset for solar maximum is shorter than for solar minimum, because there are fewer long continuous time periods of fast solar wind.

CONCLUSIONS

We have examined the scaling of velocity and magnetic field fluctuations measured in the solar wind at ~ 1 AU by ACE. We find that projecting these with respect to a locally averaged background magnetic field provides in GSF a clear indicator of the spectral break between the inertial range and "$1/f$" range of scaling. In GSF plots, the projected velocity and magnetic field fluctuations track each other closely in the inertial range in both fast and slow solar wind and at solar maximum and minimum. At longer timescales the "$1/f$" range is easily identified as the magnetic field fluctuations display a flattening of the GSFs (exponents become zero) consistent with a $\sim 1/f$ PSD. The velocity fluctuations on the other hand have GSFs which steepen, consistent with a PSD of $\sim 1/f^{\alpha}$ where α varies with conditions but is closer to two. The extent of the inertial range determined in this manner differs between fast and slow solar wind streams, and between periods of maximum and minimum solar activity. The GSF is a generic technique to determine scaling exponents and is not restricted in

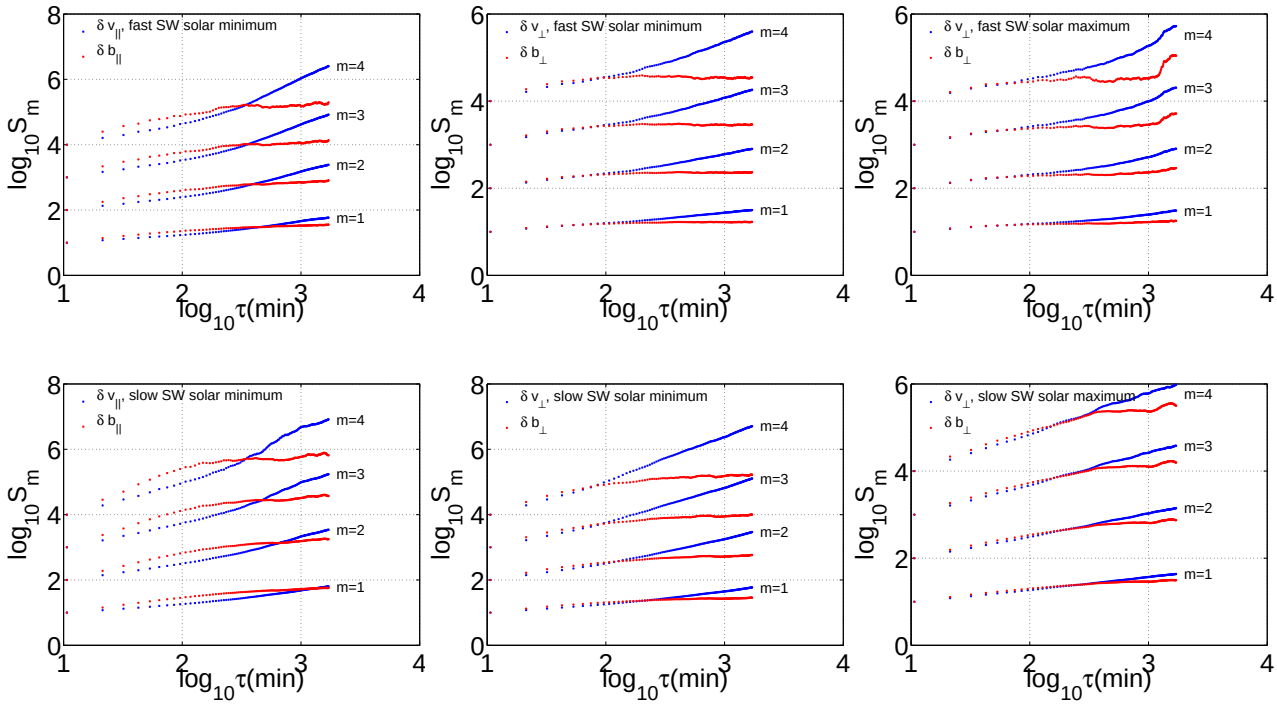

FIGURE 2. (Reproduced by permission of the AAS from [26]) GSF of fluctuations in the fast solar wind (upper) and in the slow solar wind (lower). The left and centre panels refer to the solar minimum in 2007 and plot velocity (blue) and magnetic field (red) parallel and perpendicular components respectively. The right hand panel plots perpendicular components for the solar maximum in 2000. For clarity only the 0.4% conditioned results are shown, see [26]

application to *in situ* turbulence; exponents can also be found the "$1/f$" range as has been done in [26].

ACKNOWLEDGMENTS

We acknowledge the STFC and UKAEA Culham for financial support and R. P. Lepping and the ACE team for data provision.

REFERENCES

1. Bavassano, B., Dobrowolny, M., Mariani, F., & Ness, N. F. 1982, *J. Geophys. Res.*, 87, 3617
2. Bruno, R., Carbone, V., Primavera, L., Malara, F., Sorriso-Valvo, L., Bavassano, B., & Veltri, P. 2004, *Ann. Geophys.*, 22, 3751
3. Bruno, R., & Carbone, V. 2005, Living Reviews in Solar Physics, 2, 4
4. Burlaga, L. F., & Forman, M. A. 2002, *J. Geophys. Res.*, 107, 1403
5. Chapman, S. C., Hnat, B., Rowlands, G., & Watkins, N. W. 2005, *Nonlin. Proc. Geophys.*, 12, 767
6. Chapman, S. C., & Hnat, B. 2007, *Geophys. Res. Lett.* , 34, 17103
7. Hnat, B., Chapman, S. C., Rowlands, G., Watkins, N. W., & Freeman, M. P. 2003, *Geophys. Res. Lett.*, 30, 220000
8. Hnat, B., Chapman, S. C., & Rowlands, G. 2005, *J. Geophys. Res.*, 110, 8206
9. Horbury, T., Balogh, A., Forsyth, R. J., & Smith, E. J. 1995a, *Ann. Geophys.*, 13, 105
10. Horbury, T. S., Balogh, A., Forsyth, R. J., & Smith, E. J. 1996a, *J. Geophys. Res.*, 101, 405
11. Horbury, T. S., & Balogh, A. 1997, *Nonlin. Proc. Geophys.*, 4, 185
12. Horbury, T. S., Forman, M. A., & Oughton, S. 2005, *PPCF*, 47, 703
13. Horbury, T. S., Forman, M., & Oughton, S. 2008, *Phys. Rev. Lett.*, 101, 175005
14. Kiyani, K., Chapman, S. C., & Hnat, B. 2006, *Phys. Rev. E*, 74, 051122
15. Kiyani, K., Chapman, S. C., Hnat, B., & Nicol, R. M. 2007, *Phys. Rev. Lett.*, 98, 211101
16. Marsch, E., & Tu, C.-Y. 1990a, *J. Geophys. Res.*, 95, 8211
17. Marsch, E., & Tu, C.-Y. 1990b, *J. Geophys. Res.*, 95, 11945
18. Marsch, E., & Tu, C.-Y. 1997, *Nonlin. Proc. Geophys.*, 4, 101
19. Matthaeus, W. H., & Goldstein, M. L. 1986, *Phys. Rev. Lett.*, 57, 495
20. Matthaeus, W. H., Goldstein, M. L., & Roberts, D. A. 1990, *J. Geophys. Res.*, 95, 20673
21. Matthaeus, W. H., Breech, B., Dmitruk, P., Bemporad, A., Poletto, G., Velli, M., & Romoli, M. 2007, *Ap. J. Letters* 657, L121

22. McComas, D. J., Bame, S. J., Barker, P., Feldman, W. C., Phillips, J. L., Riley, P., & Griffee, J. W. 1998, *Space Sci. Rev.*, 86, 563
23. Merrifield, J. A., Müller, W.-C., Chapman, S. C., & Dendy, R. O. 2005, *Phys. Plasmas*, 12, 022301
24. Merrifield, J. A., Chapman, S. C., & Dendy, R. O. 2007, *Phys. Plasmas*, 14, 012301
25. Nicol, R. M., Chapman, S. C., & Dendy, R. O. 2008,*Ap. J.* , 679, 862
26. Nicol, R. M., Chapman, S. C., & Dendy, R. O. 2009, *Ap. J.*, 703, 2138
27. Oughton, S., Priest, E. R., & Matthaeus, W. H. 1994, *J. Fluid Mech.*, 280, 95
28. Padhye, N. S., Smith, C. W., & Matthaeus, W. H. 2001, *J. Geophys. Res.* , 106, 18635
29. Ruzmaikin, A., Lyannaya, I. P., Styashkin, V. A., & Eroshenko, E. 1993, *J. Geophys. Res.* , 98, 13303
30. Salem, C., Mangeney, A., Bale, S. D., & Veltri, P. 2009, *Ap. J.*, 702, 537
31. Shebalin, J. V., Matthaeus, W. H., & Montgomery, D. 1983, *J. Plasma Phys.*, 29, 525
32. Smith, C. W., L'Heureux, J., Ness, N. F., Acuña, M. H., Burlaga, L. F., & Scheifele, J. 1998, *Space Sci Rev.*, 86, 613
33. Sorriso-Valvo, L., et al. 2007, *Phys. Rev. Lett.*, 99, 115001
34. Stone, E. C., Frandsen, A. M., Mewaldt, R. A., Christian, E. R., Margolies, D., Ormes, J. F., & Snow, F. 1998, *Space Sci. Rev.*, 86, 1